# Time-resolved ARPES with tunable 12–21.6 eV XUV at 400 kHz repetition rate ⊘

Famin Chen ⓘ ; Ji Wang ⓘ ; Mojun Pan ⓘ ; Junde Liu ⓘ ; Jierui Huang ⓘ ; Kun Zhao ✉ ⓘ ; Chenxia Yun ✉ ; Tian Qian ✉ ⓘ ; Zhiyi Wei ⓘ ; Hong Ding

Check for updates

View Online

Export Citation

CrossMark

AIP Publishing

# Time-resolved ARPES with tunable 12–21.6 eV XUV at 400 kHz repetition rate

View Online    Export Citation    CrossMark

Famin Chen,[1,2] ⓘ Ji Wang,[1,3] ⓘ Mojun Pan,[1,2] ⓘ Junde Liu,[1,2] ⓘ Jierui Huang,[1,2] ⓘ Kun Zhao,[1,4,a)] ⓘ
Chenxia Yun,[1,a)] ⓘ Tian Qian,[1,a)] ⓘ Zhiyi Wei,[1,2,4] ⓘ and Hong Ding[1,5]

## AFFILIATIONS

[1] Beijing National Laboratory for Condensed Matter Physics and Institute of Physics, Chinese Academy of Sciences, Beijing 100190, China
[2] University of Chinese Academy of Sciences, Beijing 100049, China
[3] School of Science, Institute of Applied Mic-Nano Materials, Beijing Jiaotong University, Beijing 100044, China
[4] Songshan Lake Materials Laboratory, Dongguan 523808, China
[5] Tsung-Dao Lee Institute, Shanghai Jiao Tong University, Shanghai 201210, China

[a)] Authors to whom correspondence should be addressed: zhaokun@iphy.ac.cn; cxyun@iphy.ac.cn; and tqian@iphy.ac.cn

## ABSTRACT

Time-resolved and angle-resolved photoemission spectroscopy (trARPES) is a powerful method to detect the non-equilibrium electronic structure in solid systems. In this study, we report a trARPES apparatus with tunable photon energy selectively among 12, 16.8, and 21.6 eV at a repetition rate of 400 kHz. The energy and temporal resolutions of the three harmonics are determined as 104/111/157 meV and 276/190/154 fs, respectively. The photon flux on the sample is estimated to be $10^{10}$–$10^{11}$ photons/s by using a photodiode. Finally, the performance of this setup is verified by both equilibrium and non-equilibrium ARPES measurements on topological materials $Zr_2Te_2P$ and $Bi_2Se_3$. Meanwhile, the importance of the tunability of the extreme ultraviolet (XUV) source is highlighted by comparing experimental results measured with the three different photon energies.

*Published under an exclusive license by AIP Publishing.* https://doi.org/10.1063/5.0143485

## I. INTRODUCTION

Angle-resolved photoemission spectroscopy (ARPES) has a unique momentum-resolved ability to study the electronic structures in materials. It is widely used in the research of unconventional superconductors,[1] topological materials,[2,3] charge-density-wave systems,[4,5] and other quantum materials.[6] In an ARPES experiment, the electrons in the materials are first kicked out by ultraviolet (UV) pulses and then collected by an electron analyzer. The UV source employed in the ARPES experiment is considered a perturbation to the system when the measured electronic spectra are analyzed. In other words, the ARPES experiments contribute to our understanding of the occupied states of equilibrium electronic structures.[7] In the past decade, the great progress of ultrafast laser and traditional ARPES technology, along with the rise of interest in studying non-equilibrium electronic structures, has stimulated the development of time-resolved ARPES (trARPES).[8–27] This new method is based on the combination of ARPES and ultrafast laser

technique. The light source used in the setup of trARPES involves two ultrafast pulses. One is typical near-infrared radiation (NIR) that acts as a pump pulse to drive the system into non-equilibrium states. The second one is UV radiation that is used to probe electronic structures. These two ultrafast pulses are coherent in the time domain, and their temporal delay $\Delta t$ can be tuned by adjusting the optical path difference. Therefore, the spectrum intensity $I(k, E)$ can be measured as a function of $\Delta t$, and a dataset containing information on system decay from non-equilibrium states can be acquired.

The NIR-UV light source used in trARPES can be generated based on nonlinear optical effect (NOE), such as the second-order NOE in nonlinear optical crystals,[8–16] or high-order harmonic generation (HHG) in noble gas.[17–27] The apparatus that uses the nonlinear optical crystal to generate probe pulse is more accessible and can help achieve high energy and temporal resolutions because the parameters of the optical crystal are tunable and the dispersion of UV or deep-UV pulse can be compensated at a reasonable

cost.[14] However, the photon energy of the probe pulse generated by using this method is typically smaller than 7 eV, resulting in a small measuring range of the Brillouin zone (BZ), usually <0.81 Å$^{-1}$, which is insufficient in most of the cases. The technique of using the tabletop laser with a photon energy of 11 eV may improve the situation,[28,29] but this photon energy is still insufficient to measure electronic structures near the boundary of the BZ, such as the cases of transition-metal dichalcogenides (TMD) or graphene. To achieve a larger measuring range of BZ, researchers have developed HHG-based apparatus and demonstrated the ability of HHG to generate coherent extreme ultraviolet (XUV) source (>20 eV) suitable for trARPES.[17–27] Such apparatus have extensive applications in the research of materials containing crucial electronic structures at the point of large momentum.[30–34] Furthermore, the HHG spectrum contains discrete harmonics with similar intensity, which in combination with a monochromator can be used to realize a tunable XUV light source.[18–20,24] Such an in-lab tunable XUV source is preferable in ARPES experiments. The cross-section of the photon-electron scattering and the penetration depth of UV pulses into materials are strongly dependent on the photon energy, and therefore, some electronic states are accessible with photon energies in a certain range.[7,35,36] This is where a tunable XUV source plays an important role.

In this paper, we report an HHG-based apparatus of trARPES. This setup can be operated with tunable probe photon energies selectively among 12, 16.8, and 21.6 eV by using a grating to isolate different harmonics. The energy and temporal resolutions of three harmonics were determined to be 104/111/157 meV and 276/190/154 fs, respectively. The photon flux was estimated to be $10^{10}$–$10^{11}$ photons/s by *in situ* measurements using a photodiode.

Finally, we show the experimental results of topological materials $Zr_2Te_2P$ and $Bi_2Se_3$ measured with this setup, demonstrating its good performance in measuring the electronic structures and tracing the dynamic process of non-equilibrium electronic states. We highlight the advantages of our trARPES setup with a discretely tunable XUV source. The three harmonics of photon energies of 12, 16.8, and 21.6 eV were optimized to be of great beam quality for ARPES measurements. Our setup provides a high photon energy of up to 21.6 eV to enable a large accessible measuring range of the BZ while giving alternatives of 12 and 16.8 eV, which may facilitate probing energy bands that are sensitive to certain photon energies.[35]

## II. trARPES SETUP

### A. Layout of XUV source based on HHG

As shown in Fig. 1, a Yb-doped fiber laser provides the fundamental beam (FB) with a wavelength of 1030 nm (h$\nu$ = 1.2 eV) at a repetition rate of 400 kHz and with output power up to 20 W. The stability of the fiber laser system is evaluated by an 8 h long-time test of average-power variation, and the measured value is less than 1% rms. A beam splitter is used to divide the beam into two, and about 90% of the total power is used for the generation of an XUV source. The efficiency of the HHG process is increased by compressing the pulse duration of FB from 40 to 25 fs by using nonlinear spectral broadening in fused silica plates and subsequent dispersion compensation by chirp mirrors.[37,38] Then, a beta barium borate (BBO) crystal with a thickness of 0.4 mm is used to double the frequency of FB, and the efficiency of the second-harmonic generation is about 30%. Subsequently, the $\omega$ and $2\omega$ beams propagate through a dual wave plate ($\lambda$/2@1030, $\lambda$@515 nm), which is used to adjust their
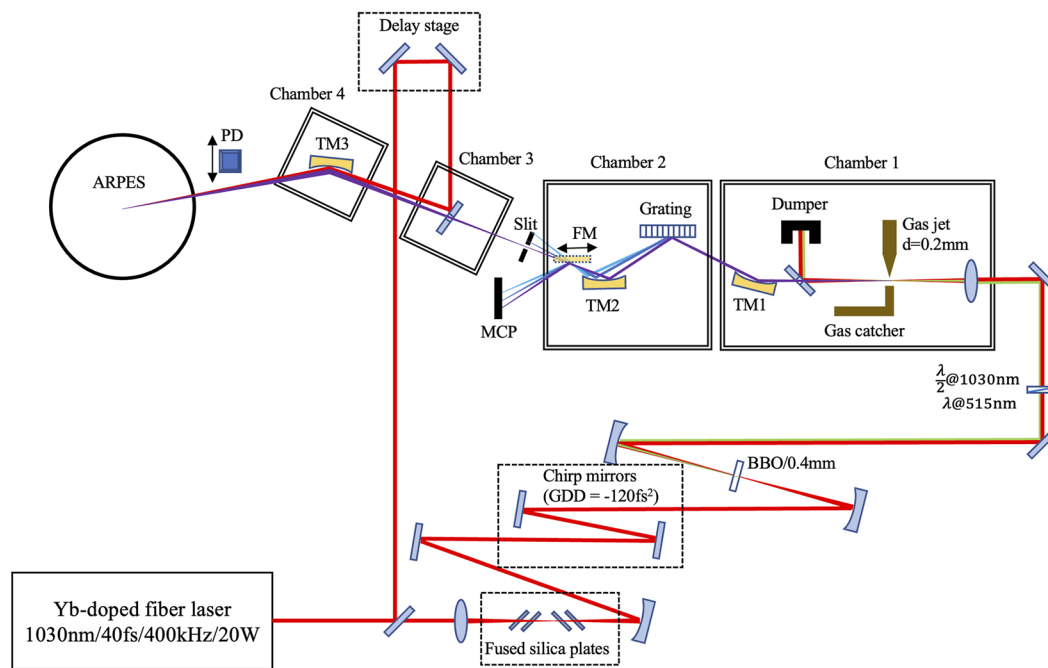
**FIG. 1.** A schematic layout of the XUV source.

polarizations, and then focus at the Krypton gas jet by a focusing lens of f = 200 mm. The gas target is a nozzle with a pore of a diameter of 200 $\mu$m, which is mounted close to a gas catcher connected to a scroll dry pump. The nozzle and the catcher are both installed on three-axis linear stages to achieve position adjustment. A reflecting mirror with a small hole in the center reflects the remaining power of $\omega$ and $2\omega$ pulses, while the generated XUV propagates through the hole and is then collimated by a toroidal mirror (TM1, f = 400 mm). In the second chamber, a single diffraction grating whose groove density is 150 gr/mm and blazing angle is 2.2° is used to isolate different harmonics, which are then focused by TM2 (f = 300 mm). A narrow slit is mounted at the focus point of TM2 between the second and third chambers, and this slit enables only one selected harmonic to propagate through it. The harmonics with different photon energies will go through the slit in sequence when the grating is sequentially rotated and then be employed in experiments. The pump beam is introduced in the third chamber and is focused on the sample using TM3 (f = 550 mm), which also plays a role in imaging the slit plane to the position of samples at the ratio of 1:1.[39,40]

## B. Design of ARPES setup

The ARPES setup consists of four chambers: load-lock chamber, pre-chamber, process chamber, and analyze chamber (Fig. 2). The process chamber is equipped with an Ar-gun to sputter the sample surface with high-energy Ar plasma and a heating stage to anneal samples. The analyze chamber has two inlets for light sources. One inlet is equipped with a helium-discharged lamp to measure the overall band structures and align the orientation of samples. The other inlet is designed for an HHG-based XUV source and a NIR source used for pump pulses. The apparatus is equipped with a six-axis manipulator and can be operated at the lowest temperature of 6 K with open cycling He-4.

The vacuum of the analyze chamber is better than $4 \times 10^{-11}$ Torr when the valve of the inlet of HHG-based XUV is closed. However, when the XUV is used in the experiments, all four chambers of the HHG setup and the analyze chamber of ARPES are connected without any valves closed. The connecting tubes are designed to be of a relatively small diameter to keep a large pressure gradient between different chambers. A turbo pump and an ion pump (pump speed of 75 l/s for $N_2$) are used in the last tube connected to the analyze chamber. The vacuums of the four chambers of the HHG setup are about $10^{-3}$, $10^{-6}$, $10^{-8}$, and $10^{-10}$ Torr. When the valve of the inlet is opened, the vacuum of the analyze chamber becomes slightly worse and is about $8 \times 10^{-11}$ Torr.

## C. Characterization of XUV source

A gold-coated flat mirror (FM) in chamber 2 (Fig. 1) is mounted in a motorized linear stage placed in front of the slit. It will reflect the focusing harmonics to the MCP detector when inserted into the beam. The image on the detector shows a series of XUV harmonics [Fig. 3(a)], of which the three harmonics exhibiting the strongest intensity are used for ARPES experiments. We mount a photodiode (PD) in a motorized linear stage before samples move it in and out of the propagating path of XUV to measure the photon flux and optimize the efficiency of HHG. By carefully adjusting the backing pressure of Kr at the gas jet, we find that the intensities of the three harmonics show different pressure dependencies [Fig. 3(b)]. Finally, this setup achieves an operating performance at a photon flux of about $10^{10}$–$10^{11}$ photons/s (Table I). The magnitude of the photon flux is normal compared with other XUV sources of trARPES based on fiber laser systems and it warrants an acceptable efficiency of data acquisition. It is worth noting that the photoelectron intensities of the same sample measured with different harmonics are similar, even though the flux of the 18th harmonic is more than twice that of the 14th harmonic. This is because the analyzer of ARPES collects photoelectrons within a small energy window near the Fermi level, while the photoelectrons distribute in the whole energy range below Fermi energy. Therefore, the collected photoelectrons will make up a larger part of the whole when the photon energy is smaller.

We evaluated the spectral characteristics of XUV by analyzing the experimental results of ARPES (Fig. 4). For this, the momentum-integrated energy distribution curves (EDC) of polycrystalline gold at 10 K are fitted by the convolution of the Fermi–Dirac distribution
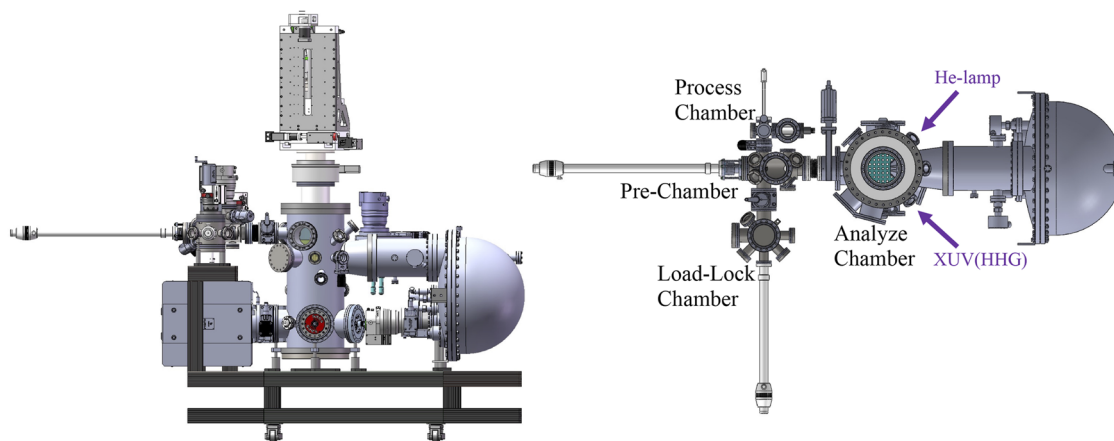
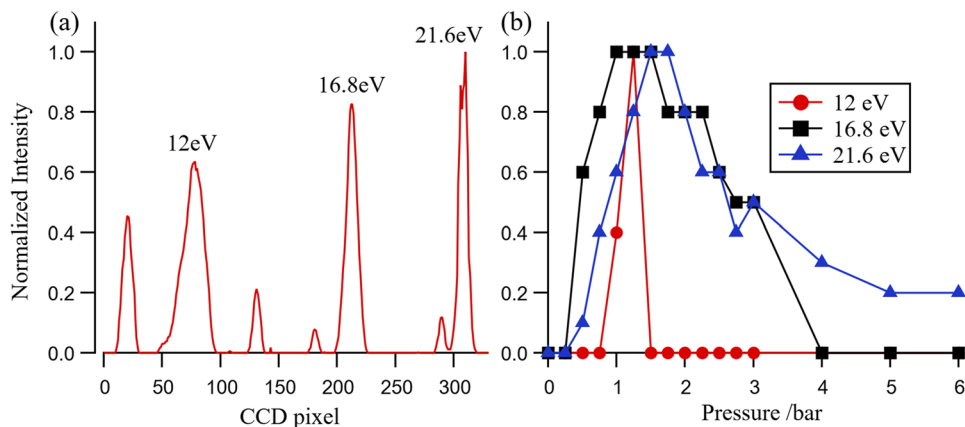**FIG. 2.** A schematic layout of ARPES.

**FIG. 3.** (a) XUV harmonics imaged by CCD after being isolated by the monochromator. (b) Pressure dependence of the efficiency of harmonics.

**TABLE I.** The parameters of the three harmonics.

| Order | $h\nu$ (eV) | $\Delta E$ (meV) | $\Delta t$ (fs) | Flux (photons/s) |
|-------|------|--------|--------|------------------|
| 10th | 12.0 | 104 | 276 | $4.8 \times 10^{10}$ |
| 14th | 16.8 | 111 | 190 | $7.2 \times 10^{10}$ |
| 18th | 21.6 | 157 | 154 | $1.1 \times 10^{11}$ |

and a Gaussian function [Fig. 4(a)] to acquire energy resolutions for the three isolated harmonics, i.e., 104/111/157 meV for the photon energies of 12/16.8/21.6 eV. The temporal resolutions are extracted from the temporal distribution curves (TDC) of the topological

insulator $Bi_2Se_3$. A product of a step function and an exponential decay function, convolved with a Gaussian envelope, is used to describe the dynamic evolution of the intensity[14] [Fig. 4(c)]. We obtain the results of 276/190/154 fs for the photon energies of 12/16.8/21.6 eV. The pulse durations of the $\omega$ and $2\omega$ pulses are 25 and 30 fs, respectively. However, the monochromator cannot preserve the pulse duration as short as in the generation process. The grating is mounted in the geometry of classical-diffraction mount (CDM), a relatively simple geometry widely used in the monochromator of XUV. The main drawback of CDM is that it introduces a stretch of pulse duration by the pulse-front tilt, resulting in worse temporal resolutions, as observed in our setup.[40,41] It is also noteworthy that the data of temporal resolutions of the three harmonics
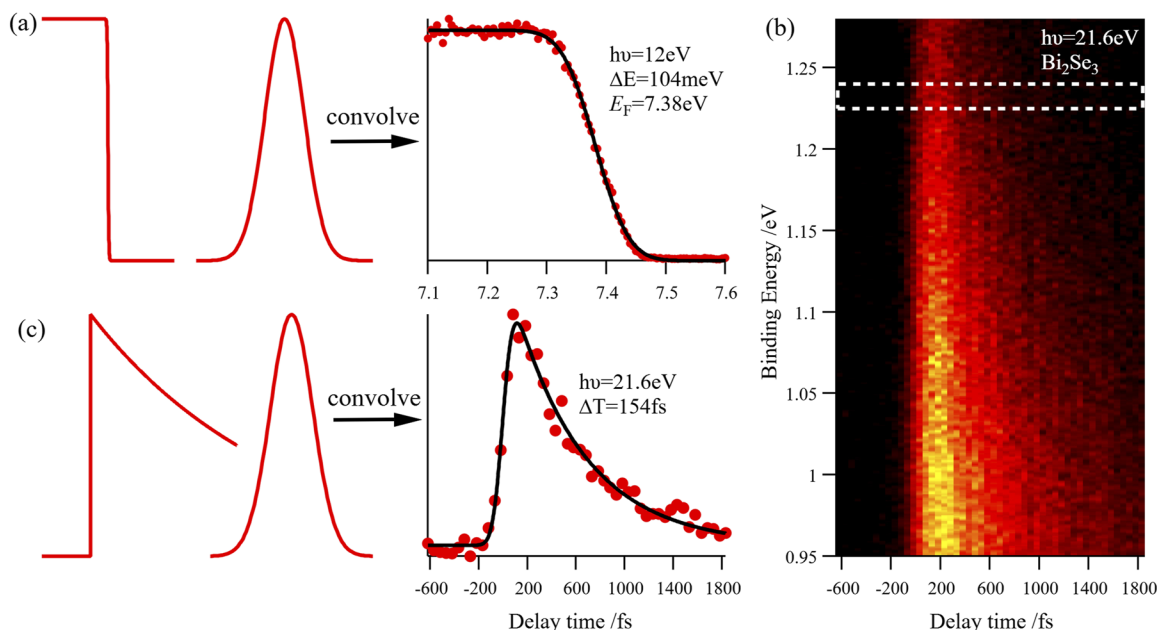


**FIG. 4.** Characterization of XUV source. (a) EDC (red dotted line) from the data of polycrystalline gold measured with the photon energy of 12 eV. The black solid line is the convolution of a Fermi–Dirac function and a Gaussian function (red solid lines). (b) Integrated EDCs of $Bi_2Se_3$ as a function of delay time measured with the photon energy of 21.6 eV. (c) TDC (red dotted line) by integrating the intensity of an energy window shown by the white dotted box in (b) and the fitting results.

were acquired by long-time experiments lasting more than 12 h. Furthermore, the dynamic measurement of $Bi_2Se_3$ described in Sec. III C (Fig. 8) took more than 5 h. The data quality shows the stability of the XUV source, which warrants its capability in time-resolved experiments.

## III. EXPERIMENTAL RESULTS MEASURED WITH HHG-BASED XUV

### A. Fermi surface mapping of $Zr_2Te_2P$

$Zr_2Te_2P$ is a topological material in the tetradymite structure family.[42] Since the stacking Te–Zr–P–Zr–Te layers are bonded by weak Van der Waals forces, the samples can be easily cleaved along the (001) plane. As shown in Fig. 5, the measured Fermi surfaces

(FSs) on the (001) plane consist of six electron-like pockets at M points and a hole-like pocket at Γ point, showing a sixfold symmetry. These clear features of the FSs demonstrate that the beam qualities of the three harmonics are sufficiently good for ARPES experiments. Meanwhile, the FS mapping results show a larger measuring range of BZ for the higher photon energy under the same experimental configuration, which is more than 50% of expansion when the result of 21.6 eV [Fig. 5(c)] is compared to that of 12 eV [Fig. 5(a)]. The maximum of the in-plane component of the momentum can be theoretically determined as $k_\parallel = \sqrt{2mE_{kin}}/\hbar$, where $E_{kin}$ is the kinetic energy of photoelectrons. When the probe photon energy is 21.6 eV, the theoretical maximum value of $k_\parallel$ at $E = E_F$ is about 2.1 Å$^{-1}$, which is enough to measure the electronic structures on the boundary of the BZ for almost all the materials.



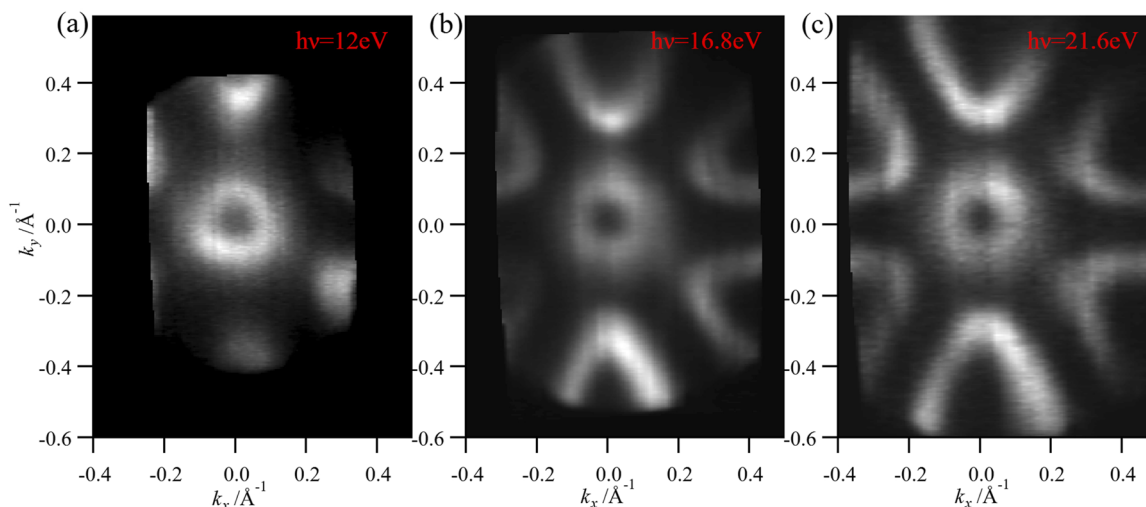**FIG. 5.** (a)–(c) The ARPES intensity plot at $E - E_F$ of topological metal $Zr_2Te_2P$ measured with a photon energy of 12/16.8/21.6 eV. The intensity is acquired by integrating over an energy window of 20 meV.
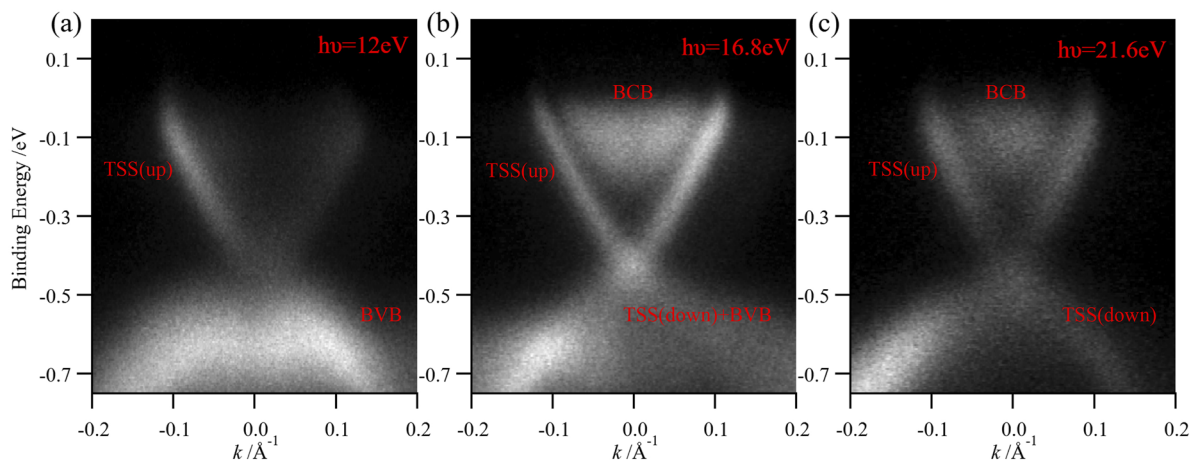


**FIG. 6.** (a)–(c) The band structures of $Bi_2Se_3$ near Γ point measured with a photon energy of 12/16.8/21.6 eV.

## B. Band structure of Bi₂Se₃

$Bi_2Se_3$ is a well-known topological insulator[43] and is used to highlight the importance of photon energy tunability. The features of bulk valence bands (BVB), bulk conducting bands (BCB), and topological surface states (TSS) show a significant dependence on photon energies. The M-shape feature of the BVB is clearly detected by using the photon energy of 12 eV [Fig. 6(a)], but is gradually mixed with the down branch of TSS when $h\nu$ = 16.8 eV [Fig. 6(b)], and, finally, is completely invisible when $h\nu$ = 21.6 eV [Fig. 6(c)]. On the contrary, the BCB signature is absent in the spectrum measured with a photon energy of 12 eV, whereas it is clearly visible in the results of the other two harmonics. Finally, the up branch of TSS can be seen in all three spectra, but the one of $h\nu$ = 16.8 eV has an advantage of a higher signal-to-noise ratio and shaper peak feature. These differences are due to the photon energy dependence of electron-photon scattering cross-section, or the distinct out-of-plane momentum $k_z$. We emphasize the importance of photon energy tunability, especially the alternative of relatively lower photon energies of 12 and 16.8 eV. These two harmonics are preferable in some cases, such as for researchers who care more about the feature of the TSS, which are generally believed to be more sensitive to lower photon energies.

## C. trARPES results of Bi₂Se₃

We choose the harmonic of $h\nu$ = 16.8 eV for the time-resolved experiment of $Bi_2Se_3$. Figure 7(b) shows the experimental results of $Bi_2Se_3$ at four different delay times of t = −5/0.2/1/5 ps. The intensity above $E_F$ is scaled exponentially as a function of $E − E_F$ while the one below $E_F$ is kept unchanged in order to ensure the visibility of all the characteristics of the band structure in the same image. The

dynamic process of the non-equilibrium electrons of $Bi_2Se_3$ is illustrated by using a simplified schematic shown in Fig. 7(a) and is also demonstrated by the non-equilibrium band structures measured by trARPES [Fig. 7(b)]. As observed, the electrons are first excited to high energy states in a short time, then gradually decay to the low energy states of the BCB and of the TSS, and finally drop back to the states of the BVB. The inter-band scattering between the BVB and BCB is mediated by the TSS. Therefore, the small density of the TSS will limit the decay process and result in a relatively long lifetime of the non-equilibrium electrons in $Bi_2Se_3$.[44]

We analyzed the temporal distribution of the integrated intensity of four different energy windows [Fig. 8(a): $E − E_F$ = 50–100; 100–150; 150–200; 200–250 meV] in detail. The TDCs are fitted by a Gaussian function convolved with the product of the step function and the single-exponential function,

$$I(t) = A\left(1 + \text{erf}\left(\frac{t - t_0}{\Delta t}\right)\right)e^{-\frac{t-t_0}{\tau}} + B, \quad (1)$$

where $\Delta t$ is the width of the Gaussian envelope, and $\tau$ is the decay parameter of the single-exponential function.[14] The above formula ignores the filling process from higher energy states to lower energy states and is, thus, suitable only for the TDCs of states far above $E_F$. However, this expression is sufficient to depict the dynamic evolution of the four TDCs smoothly. We normalized the smooth-fitting curves and draw them together in Fig. 8(b). Our results showed that the transient intensity of higher energy states needs a shorter time to reach the maximum and to decay to the equilibrium status, as expected. Finally, we fit the TDCs after 2 ps with the single-exponential decay function to extract the lifetime of excited electrons. These electrons have a longer lifetime at lower binding energy, as long as several picoseconds [Fig. 8(c)], in agreement with the results of previous studies.[43–46]
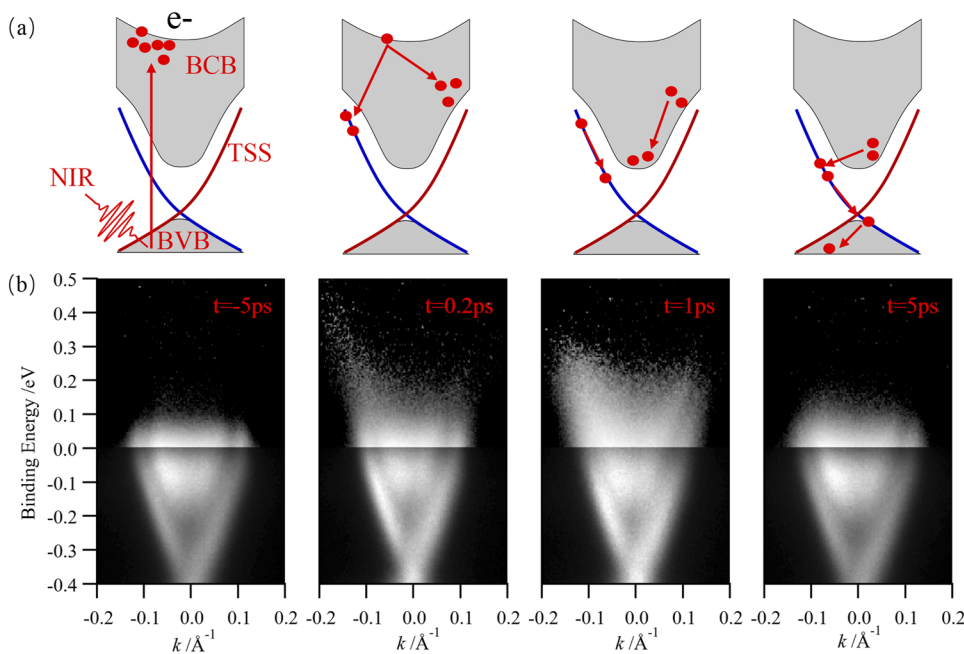


**FIG. 7.** (a) Schematic of the transitions and scattering processes in trARPES experiments of $Bi_2Se_3$.[44] To simplify the schematic, only the direct optical transition from the BVB is considered. (b) Non-equilibrium states of $Bi_2Se_3$ measured at t = −5/0.2/1/5 ps at 30 K, using the photon energy of 16.8 eV.
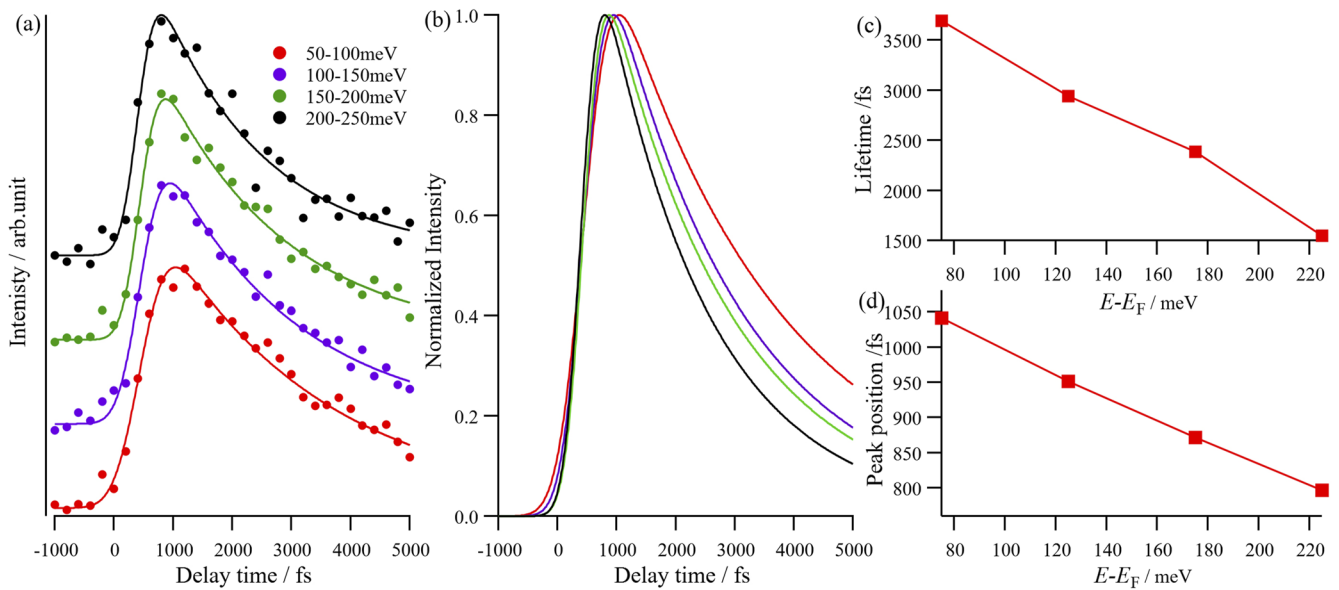
**FIG. 8.** (a) Transient photoemission intensities at the energy windows of (50–100)/(100–150)/(150–200)/(200–250) meV (solid dots) and the four fitting curves (solid lines). The intensity is acquired by integrating the whole angle range and a 50 meV energy window. The lines are shifted for exhibition. (b) The normalized fitting curves from (a). (c) The lifetimes extracted by fitting the decay data with an exponential decay function. (d) The peak positions of curves in (b).

## IV. CONCLUSION

In summary, we report an HHG-based trARPES setup with a tunable XUV source, which can be operated at the photon energies of 12, 16.8, and 21.6 eV. The energy and temporal resolutions are 104/111/157 meV and 276/190/154 fs, respectively, for the three harmonics. The resolutions may be improved to sub-100 meV and sub-100 fs in the future if we redesign the monochromator to compress the pulse duration stretch of XUV introduced by pulse-front tilt. The measured photon flux is about $10^{10}$–$10^{11}$ photons/s, which may be improved in future work by driving the HHG with a two-color field. Finally, the capability of this setup is verified by experiments of topological materials $Zr_2Te_2P$ and $Bi_2Se_3$, and it is demonstrated to be an effective method to study the electronic structures in both static and dynamic experiments. We stress the advantage of discrete tunability from a low photon energy of 12 eV to the highest one of 21.6 eV. Such a tunability of photon energies is preferred in the ARPES experiment and its importance has been partially revealed by comparing experimental results of $Zr_2Te_2P$ and $Bi_2Se_3$ measured with the three different photon energies.

## AUTHOR DECLARATIONS

### Conflict of Interest

The authors have no conflicts to disclose.

### Author Contributions

H.D. and Z.W. provided the project direction. T.Q., C.Y., and K.Z. were the supervisors. F.C., J.W., M.P., and J.L. designed and built the setup. F.C. performed the experiments, analyzed the data, and wrote the main manuscript with the help of J.H.

**Famin Chen**: Data curation (equal); Investigation (equal); Software (equal); Writing – original draft (equal); Writing – review & editing (equal). **Ji Wang**: Data curation (equal); Investigation (equal). **Mojun Pan**: Data curation (equal); Investigation (equal); Software (equal). **Junde Liu**: Data curation (equal); Investigation (equal); Software (equal). **Jierui Huang**: Data curation (supporting); Investigation (supporting); Writing – review & editing (equal). **Kun Zhao**: Conceptualization (equal); Project administration (equal); Supervision (equal). **Chenxia Yun**: Conceptualization (equal); Project administration (equal); Supervision (equal). **Tian Qian**: Conceptualization (equal); Project administration (equal); Supervision (equal); Writing – review & editing (equal). **Zhiyi Wei**: Conceptualization (equal); Funding acquisition (equal); Project administration

(equal). **Hong Ding**: Conceptualization (equal); Funding acquisition (equal); Project administration (equal); Supervision (equal).

## DATA AVAILABILITY

The data that support the findings of this study are available from the corresponding author upon reasonable request.

## REFERENCES

[1] A. Damascelli, Z. Hussain, and Z.-X. Shen, Rev. Mod. Phys. **75**, 473 (2003).

[2] M. Z. Hasan and C. L. Kane, Rev. Mod. Phys. **82**, 3045 (2010).

[3] B. Q. Lv, T. Qian, and H. Ding, Rev. Mod. Phys. **93**, 025002 (2021).

[4] V. Brouet, W. L. Yang, X. J. Zhou, Z. Hussain, R. G. Moore, R. He, D. H. Lu, Z. X. Shen, J. Laverock, S. B. Dugdale, N. Ru, and I. R. Fisher, Phys. Rev. B **77**, 235104 (2008).

[5] P. Chen, Y.-H. Chan, X.-Y. Fang, Y. Zhang, M.-Y. Chou, S.-K. Mo, Z. Hussain, A.-V. Fedorov, and T.-C. Chiang, Nat. Commun. **6**, 8943 (2015).

[6] H. Yang, A. Liang, C. Chen, C. Zhang, N. B. M. Schroeter, and Y. Chen, Nat. Rev. Mater. **3**, 341 (2018).

[7] S. Hüfner, *Photoelectron Spectroscopy: Principles and Applications* (Springer Science and Business Media, 2013).

[8] E. Carpene, E. Mancini, C. Dallera, G. Ghiringhelli, C. Manzoni, G. Cerullo, and S. De Silvestri, Rev. Sci. Instrum. **80**, 055101 (2009).

[9] C. L. Smallwood, C. Jozwiak, W. Zhang, and A. Lanzara, Rev. Sci. Instrum. **83**, 123904 (2012).

[10] F. Boschini, H. Hedayat, C. Dallera, P. Farinello, C. Manzoni, A. Magrez, H. Berger, G. Cerullo, and E. Carpene, Rev. Sci. Instrum. **85**, 123903 (2014).

[11] Y. Ishida, T. Togashi, K. Yamamoto, M. Tanaka, T. Kiss, T. Otsu, Y. Kobayashi, and S. Shin, Rev. Sci. Instrum. **85**, 123904 (2014); arXiv:1612.04910.

[12] Y. Ishida, T. Otsu, A. Ozawa, K. Yaji, S. Tani, S. Shin, and Y. Kobayashi, Rev. Sci. Instrum. **87**, 123902 (2016); arXiv:1612.03026.

[13] Y. Yang, T. Tang, S. Duan, C. Zhou, D. Hao, and W. Zhang, Rev. Sci. Instrum. **90**, 063905 (2019); arXiv:2003.00515.

[14] C. Bao, L. Luo, H. Zhang, S. Zhou, Z. Ren, and S. Zhou, Rev. Sci. Instrum. **92**, 033904 (2021).

[15] C. Yan, E. Green, R. Fukumori, N. Protic, S. H. Lee, S. Fernandez-Mulligan, R. Raja, R. Erdakos, Z. Mao, and S. Yang, Rev. Sci. Instrum. **92**, 113907 (2021); arXiv:2109.13075.

[16] C. Bao, H. Zhong, S. Zhou, R. Feng, Y. Wang, and S. Zhou, Rev. Sci. Instrum. **93**, 013902 (2022); arXiv:2112.09370.

[17] S. Mathias, L. Miaja-Avila, M. M. Murnane, H. Kapteyn, M. Aeschlimann, and M. Bauer, Rev. Sci. Instrum. **78**, 083105 (2007).

[18] G. L. Dakovski, Y. Li, T. Durakiewicz, and G. Rodriguez, Rev. Sci. Instrum. **81**, 073108 (2010).

[19] B. Frietsch, R. Carley, K. Döbrich, C. Gahl, M. Teichmann, O. Schwarzkopf, P. Wernet, and M. Weinelt, Rev. Sci. Instrum. **84**, 075106 (2013).

[20] S. Plogmaker, J. A. Terschlüsen, N. Krebs, M. Svanqvist, J. Forsberg, U. B. Cappel, J.-E. Rubensson, H. Siegbahn, and J. Söderström, Rev. Sci. Instrum. **86**, 123107 (2015).

[21] G. Rohde, A. Hendel, A. Stange, K. Hanff, L.-P. Oloff, L. X. Yang, K. Rossnagel, and M. Bauer, Rev. Sci. Instrum. **87**, 103102 (2016).

[22] J. Schmidt, A. Guggenmos, S. H. Chew, A. Gliserin, M. Högner, M. F. Kling, J. Zou, C. Späth, and U. Kleineberg, Rev. Sci. Instrum. **88**, 083105 (2017).

[23] J. H. Buss, H. Wang, Y. Xu, J. Maklar, F. Joucken, L. Zeng, S. Stoll, C. Jozwiak, J. Pepper, Y.-D. Chuang, J. D. Denlinger, Z. Hussain, A. Lanzara, and R. A. Kaindl, Rev. Sci. Instrum. **90**, 023105 (2019); arXiv:1811.00715.

[24] A. K. Mills, S. Zhdanovich, M. X. Na, F. Boschini, E. Razzoli, M. Michiardi, A. Sheyerman, M. Schneider, T. J. Hammond, V. Süss, C. Felser, A. Damascelli, and D. J. Jones, Rev. Sci. Instrum. **90**, 083001 (2019); arXiv:1902.05997.

[25] M. Puppin, Y. Deng, C. W. Nicholson, J. Feldl, N. B. M. Schröter, H. Vita, P. S. Kirchmann, C. Monney, L. Rettig, M. Wolf, and R. Ernstorfer, Rev. Sci. Instrum. **90**, 023104 (2019); arXiv:1811.06939.

[26] K. Bühlmann, R. Gort, A. Fognini, S. Däster, S. Holenstein, N. Hartmann, Y. Zemp, G. Salvatella, T. U. Michlmayr, T. Bähler, D. Kutnyakhov, K. Medjanik, G. Schönhense, A. Vaterlaus, and Y. Acremann, Rev. Sci. Instrum. **91**, 063001 (2020).

[27] M. Keunecke, C. Möller, D. Schmitt, H. Nolte, G. S. M. Jansen, M. Reutzel, M. Gutberlet, G. Halasi, D. Steil, S. Steil, and S. Mathias, Rev. Sci. Instrum. **91**, 063905 (2020); arXiv:2003.01602.

[28] Y. He, I. M. Vishik, M. Yi, S. Yang, Z. Liu, J. J. Lee, S. Chen, S. N. Rebec, D. Leuenberger, A. Zong, C. M. Jefferson, R. G. Moore, P. S. Kirchmann, A. J. Merriam, and Z.-X. Shen, Rev. Sci. Instrum. **87**, 011301 (2016); arXiv:1509.01311.

[29] C. Lee, T. Rohwer, E. J. Sie, A. Zong, E. Baldini, J. Straquadine, P. Walmsley, D. Gardner, Y. S. Lee, I. R. Fisher, and N. Gedik, Rev. Sci. Instrum. **91**, 043102 (2020); arXiv:1910.14068.

[30] F. Schmitt, P. S. Kirchmann, U. Bovensiepen, R. G. Moore, L. Rettig, M. Krenz, J.-H. Chu, N. Ru, L. Perfetti, D. H. Lu *et al.*, Science **321**, 1649 (2008).

[31] X. Shi, W. You, Y. Zhang, Z. Tao, P. M. Oppeneer, X. Wu, R. Thomale, K. Rossnagel, M. Bauer, H. Kapteyn *et al.*, Sci. Adv. **5**, eaav4449 (2019).

[32] J. Madéo, M. K. L. Man, C. Sahoo, M. Campbell, V. Pareek, E. L. Wong, A. Al-Mahboob, N. S. Chan, A. Karmakar, B. M. K. Mariserla *et al.*, Science **370**, 1199 (2020).

[33] X. Shi, W. You, Y. Zhang, Z. Tao, Y. Zhong, P. M. Oppeneer, X. Wu, R. Thomale, K. Rossnagel, M. Bauer *et al.*, in *International Conference on Ultrafast Phenomena* (Optical Society of America, 2020) p. Tu3B.4.

[34] O. Karni, E. Barré, V. Pareek, J. D. Georgaras, M. K. L. Man, C. Sahoo, D. R. Bacon, X. Zhu, H. B. Ribeiro, A. L. O'Beirne *et al.*, Nature **603**, 247 (2022).

[35] Y. J. Chen, L. X. Xu, J. H. Li, Y. W. Li, H. Y. Wang, C. F. Zhang, H. Li, Y. Wu, A. J. Liang, C. Chen, S. W. Jung, C. Cacho, Y. H. Mao, S. Liu, M. X. Wang, Y. F. Guo, Y. Xu, Z. K. Liu, L. X. Yang, and Y. L. Chen, Phys. Rev. X **9**, 041040 (2019); arXiv:1907.05119.

[36] X. Zhou, S. He, G. Liu, L. Zhao, L. Yu, and W. Zhang, Rep. Prog. Phys. **81**, 062101 (2018); arXiv:1804.04473.

[37] P. He, Y. Liu, K. Zhao, H. Teng, X. He, P. Huang, H. Huang, S. Zhong, Y. Jiang, S. Fang *et al.*, Opt. Lett. **42**, 474 (2017).

[38] Y. Gao, X. Wang, X. Zhu, K. Zhao, H. Liu, Z. Wang, S. Fang, and Z. Wei, Phys. Rev. Res. **4**, 013035 (2022).

[39] S. Xu, J. Wang, Y. Gao, C. Yun, K. Zhao, J. Zhu, S. Fang, and Z. Wei, "Generation of 1.9-cycle pulses with 400 kHz repetition rate at 1030 nm by two-stage solid thin plates" (unpublished).

[40] J. Wang, F. Chen, M. Pan, S. Xu, R. Lv, J. Liu, Y. Li, S. Fang, Y. Chen, J. Zhu *et al.*, Opt. Express **31**, 9854 (2023).

[41] L. Poletto and F. Frassetto, Appl. Sci. **3**, 1 (2012).

[42] H. Ji, I. Pletikosić, Q. D. Gibson, G. Sahasrabudhe, T. Valla, and R. J. Cava, Phys. Rev. B **93**, 045315 (2016); arXiv:1512.00528.

[43] H. Zhang, C.-X. Liu, X.-L. Qi, X. Dai, Z. Fang, and S.-C. Zhang, Nat. Phys. **5**, 438 (2009).

[44] J. A. Sobota, S. Yang, J. G. Analytis, Y. L. Chen, I. R. Fisher, P. S. Kirchmann, and Z.-X. Shen, Phys. Rev. Lett. **108**, 117403 (2012).

[45] Y. H. Wang, D. Hsieh, E. J. Sie, H. Steinberg, D. R. Gardner, Y. S. Lee, P. Jarillo-Herrero, and N. Gedik, Phys. Rev. Lett. **109**, 127401 (2012).

[46] A. Crepaldi, B. Ressel, F. Cilento, M. Zacchigna, C. Grazioli, H. Berger, P. Bugnon, K. Kern, M. Grioni, and F. Parmigiani, Phys. Rev. B **86**, 205133 (2012).

18 July 2023 03:20:17